Development and Optimisation of a PLA Bio-based Feedstock for PIM-like Extrusion-based Additive Manufacturing (EAM) of Tool Steel Alloy

CHARPENTIER Nicolas[1] nicolas.charpentier@femto-st.fr; BOUDEAU Nathalie[1] nathalie.boudeau@ens2m.fr; BARRIERE Thierry[1] thierry.barriere@femto-st.fr; BERNARD Frederic[2] frederic.bernard@u-bourgogne.fr; VIKNER Peter[3] peter.vikner@eramet.com;

[1] (FEMTO-ST Institute, CNRS/UFC/ENSMM/UTBM, Department of Applied Mechanics, 24 chemin de l'Epitaphe, 25000 Besançon, France)
[2] (Laboratoire ICB - UMR 6303 CNRS/UBFC, 9 Avenue Alain Savary BP 47870, Dijon, 21078, France)
[3] (Aubert & Duval, Rue du Villa, 63770 Les Ancizes, France)

Abstract

Bio-based binder alleviate the important carbon footprint that is created during PIM-like process with a carbon cycle for the binder. Moreover, some bio-based polymers are more suited to EAM, like PLA.
This work presents the different steps in developing a suitable pellets feedstock for PIM-like EAM and its optimisation to minimize porosity. This latter is controlled by tomographic observation in the final part. The work is focused on the use of a tool steel alloy powder but using the same method other materials can broaden the field of application.
PIM-like Extrusion-based Additive Manufacturing allow an increase in complexity of shape, and an ease of use, not needing tooling to produce parts. The production of a specific feedstock, and not using PIM feedstock, provides a better mastery of the process. Moreover, this work provides additional knowledge into bio-based feedstocks.

Main text

1. Introduction

Powder Injection Moulding (PIM) involves the use of a feedstock (a mix of a polymeric binder and a powder load) in an injection moulding process. The conventional thermoplastic polymers used are polypropylene, polyethylene or polyacetal [1]. Royer et al. in [2] proposed to employ some bio sourced polymers as binder and especially PLA. In order to obtain the homogeneous feedstock with high powder volume loading, some surfactants are used such as stearic acid (SA) or paraffin wax, the former being a natural component extracted from vegetal oil [1]. The advantage of injection moulding process is to obtain 3D complex shape in high volume production. The part produced, qualified as green can be used as a composite material or follow a process to transform the part in order to obtain the quality of the load material. The debinding stage consist in eliminating the polymer by thermal degradation or chemical decomposition [1]. Finally, the densification stage is realized by solid state diffusion with conventional sintering [1]. PIM is a mature process with a wide range of materials at disposal such as stainless steel, titanium, superalloys.

Extrusion-based Additive Manufacturing (EAM) [3] is the controlled extrusion of a viscous material through a nozzle combined with the relative movement of said nozzle to create a geometry, combined layer by layer. This additive method of production has the advantage of not needing tooling and the ability to produce highly complex shapes. EAM has the downside of being a slow process and producing parts that have lower mechanical properties than conventional manufacturing. This process is widely available for thermoplastic polymers such as polylactic acid (PLA) or acrylonitrile butadiene styrene (ABS). Combined with a solid powder load, the viscous material can be used as a vector of shape. EAM contains two sub-methods according to the viscosity of the matter: slurry obtained with liquid are used in robocasting [4], while feedstock obtained with polymers are used in 3D printing [5-7].

Combined EAM and PIM processes can be employed to produce highly complex and low-cost full dense components in metals or ceramics [8]. This hybrid process has recently been applied to powder forming process with metallic powders such as 17-4 PH or 316L [9-10]. One advantage of PIM-like EAM over Laser Powder Bed Fusion is that, as the material is not remelted, it is possible to process difficult to weld materials such as high carbon tool steels and intermetallic alloys [2]. The final metallic components are characterized by high density and homogeneous microstructure. The mechanical properties are close to those of materials produced by traditional routes.

This article presents the process using a bio-based polymer binder formulation to shape a tool steel alloy powder for high performance tools [11], that will be debinded with thermal degradation [12] and densified by natural sintering [6;13]. In section 2, the feedstock elaboration will be described. In section 3, the combined EAM and PIM process will be developed and investigated. The EAM process used is with special printing equipment that uses granules instead of a wire. The result of the tomographic analysis of debinded and densified parts will be analysed to investigate the porosity.

2. Feedstock elaboration

2.1 Powder

The powder used is a tool steel alloy of composition X 1,28 W Mo Cr V 6-5-4-3 and commercially available under the designation ASP2023. It is transformed into a powder by gas atomization and sieved with a 63µm mesh. Table 1 show its different characteristics, measured by helium pycnometry, dilatometry, specific surface analysis and laser diffraction granulometry, respectively with a ACCUPYC II 1340 V2.00 pycnometer, a Setsys SETARAM dilatometer, a MICROMERITICS Specific Surface Analyser and a HORIBA Scientific LA-960V2 Laser diffraction particle size analyser.

Table 1. Powder characteristics

Component	Role	Melting temperature (°C)	Volumetric mass ($g \cdot cm^{-3}$)	d50 (µm)	d90 (µm)	Ss ($m^2 \cdot g^{-1}$)	Cu	Sw
ASP2023	Powder	1265±5	8,03±0,01	35,9	64,7	0,0401	1,141	3.962

The dilatometry shows that the sintering of the powder will take place between 1250°C and 1265°C, at a temperature lower than the melting temperature. Exceeding this temperature will cause a collapse of the geometry due to start of melting.

The powder granulometry, expressed with the d50 and d90 corresponding to the size at which 50% of the grains and 90% of the grain have been measured in increasing order of size, shows that while sieved with a 63 µm mesh, less than 90% of the powder (in number of grains) has a lower size than the mesh. This indicates that the grains are not totally spherical and can pass in the sieve at a certain angle and be measured at another angle showing a larger size.

The powder granulometry is used to determine the Coefficient of Uniformity (Cu) and the Slope parameter (Sw). A Cu lower than 6 indicates that the powder presents a uniform distribution, meaning that the powder grain size is centred around a single value, a Sw lower than 2 indicates that the powder has a large distribution meaning that the powder grain size is spread guaranteeing that the powder is fluid. The Specific surface (Ss) indicates the real surface area of a powder for a given quantity of it.

2.2 Binder

The feedstock is elaborated with a bio-based binder composed of a PLA and SA. Both these components are bio-based, and largely known and mastered. The SA is not weighed to obtain a particular surfactant concentration but at a fix 10%vol. in the binder. In [14], Hanemann and Heldele showed that a surfactant concentration higher than 2,2 mg/m^2 has no influence for a LDPE-SA-Paraffin wax binder, and the relatively low specific surface of the powder used guarantee that the surfactant concentration will be far higher than this rate.

The binder components are described in table 2.

Table 2. Binder components

Component	Role	Melting temperature (°C)	Volumetric mass ($g.cm^{-3}$)	Proportion in binder (%vol.)	Ref
PLA	Backbone	178 ± 1	1,25	90	[7]
SA	Surfactant	72 ± 1	0,94	10	[14]

The melting temperature is measured with a Differential Scanning Calorimetry (DSC) analysis with a DSC 31 evo SETARAM. The mix of both components in the binder leads to a modification of the melting temperature: the SA melts in the binder at 67±1°C and the PLA at 165±1°C.

2.3 Feedstock elaboration

To ensure suitable feedstock characteristics, a homogeneous feedstock is necessary, but a feedstock with the highest powder load is preferred for the sintering step (ensuring the lowest retraction). The incremental mixing method is the reference experiment to determine the suitable powder loading rate optimized by these two parameters, and is a reference method to determine this rate, as used in [15-16].

It consists in gradually increasing the powder load from a low loaded mix and observing the torque at stabilisation. By graphing the stabilised torque vs the powder load, two curves can be extracted defining the binder excess zone, the critical load, the powder-binder inhomogeneous zone and the maximal load.

In figure 1 the incremental mixing of the binder-powder is presented, where the two curves can be observed. The incremental mixing is realised in a BRABENDER Plastograph EC W50EHT.

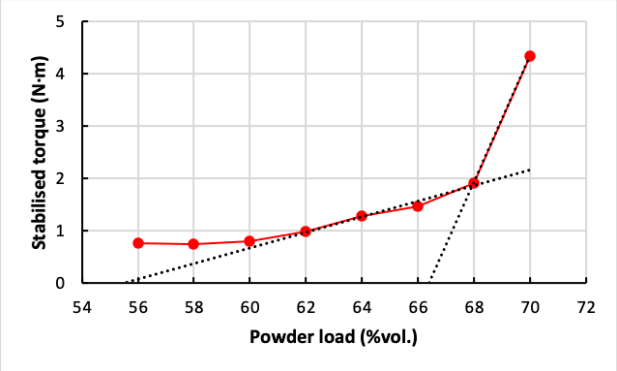

Figure 1. Incremental mixing of the feedstock, at 180°C and 30 rpm.

The two curves cross at 68%vol. in powder, indicating the critical load. Feedstock is produced at this powder load, and then granulated to be used in the further steps.

Commenté [CK1]: The two lines cross at around 67%vol? Why 70%vol?

2.4 Feedstock characterisation

The feedstock is defined but for a better understanding, a modelling may be implemented. A rheological model can be built with rheological test, with a shear rate boundary from 10 s^{-1} to 1000 s^{-1}, as EAM create typically a shear rate of 100 s^{-1}. A BOHLIN INSTRUMENTS RH2000 Capillary rheometer with a Ø2 mm die is used to measure the viscosity according to the imposed shear rate. Two temperatures of 200°C and 210°C are used to build the model according to both the shear rate and the temperature. Results are presented in figure 2.

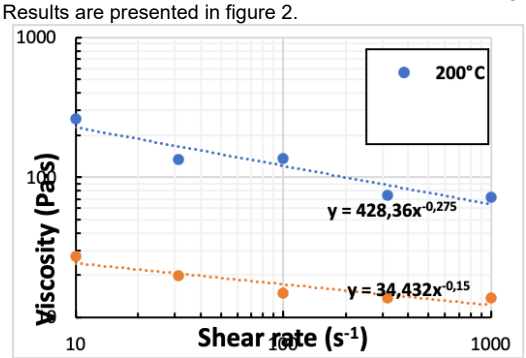

Figure 2. Capillary rheometer measurement for the feedstock loaded with 68%vol. of powder

The data show that the feedstock behaviour follows a power law, expressed as:

$$\{1\} \quad \eta(\dot{\gamma}) = K \cdot \dot{\gamma}^{n-1}$$

with η the viscosity in Pa·s, $\dot{\gamma}$ the shear rate in s-1, the constants k in Pa·s and n without unit.

The behaviour of the polymer vs the temperature can be described with the Arrhenius law, expressed as:

$$\{2\} \quad \eta(T) = B \cdot e^{\frac{E_a}{T \cdot R}}$$

with B a constant in Pa·s, R the molar gas constant at 8,314 J·K·mol^{-1}, T the temperature in Kelvin and E_a the activation energy in J·mol^{-1}.

The Arrhenius law parameters can be found by plotting the logarithm of the viscosity vs the invers of the temperature, as shown in figure 3.

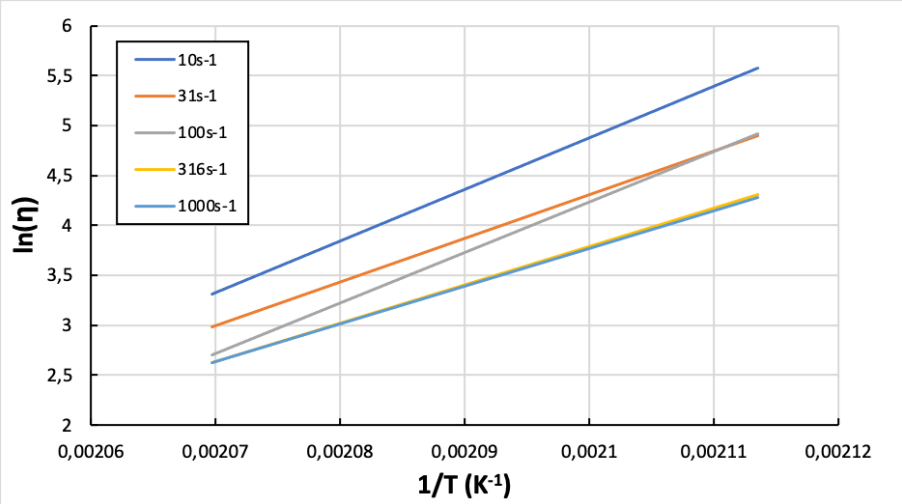

Figure 3. Logarithmical viscosity vs Invers temperature for each shear rate.

The parameters expressed in figure 3 allow us to model the Arrhenius law.
The combined power-Arrhenius law, expressed as:

$$\{3\} \quad \eta(\dot{\gamma}, T) = K \cdot \dot{\gamma}^{n-1} \cdot e^{\frac{E_a}{T \cdot R}}$$

has the parameters defined in table 3.

Table 3. Model parameters

Temperature	E_a (J·mol^{-1})	K (Pa·s)	n
200°C	361,95	428	0,7252
210°C	361,95	125	0,7572

The model is compared to the measurement in figure 4.

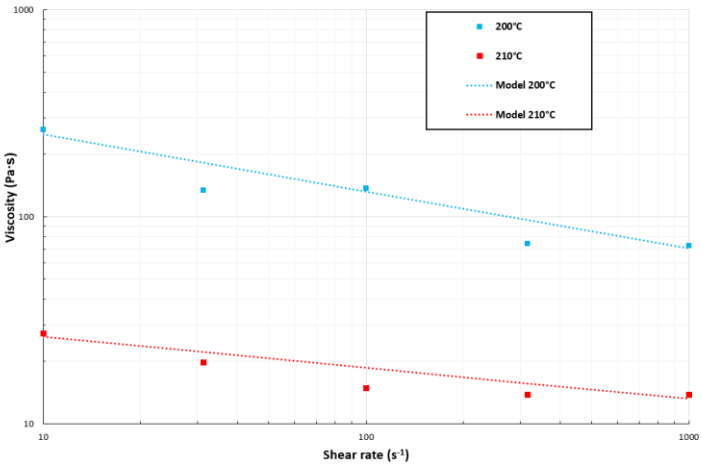

Figure 4. Rheological model vs measurement

The model constructed is an agreement with the experimental data since a low difference is observed.

3. EAM process

3.1 Printing

The printing step corresponds to the shaping of the feedstock and produces a green part. The selected geometry is a Ø8 mm by 8 mm cylinder. The small scale ensures both the possibility to sinter the part in a dilatometer and the ability for X-ray's tomograph to penetrate the part.
The printing is done with a granulate 3D printer from 3D STUDIO.
Different print parameters are used to produce a porosity-less and a low-porosity parts.

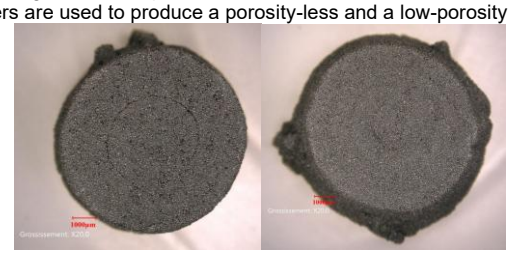

Figure 5. Top view of a cylinder printed with a) low porosity and b) no porosity

The measured porosity is equivalent to 0.03% for the no porosity samples and to 0,88% for the low porosity sample. On the figure 5, we can see the difference in porosity as the layers are barely visible in the low porosity sample but not visible at all in the no porosity sample.
A tomographic reconstruction created with an EASYTOM RX Solution tomograph of the sample is visible on figure 6. The pores are colorized according to their volume read on the left scale.

Commenté [CK2]: This is higher than for the sample with porosity? Could you explain this?

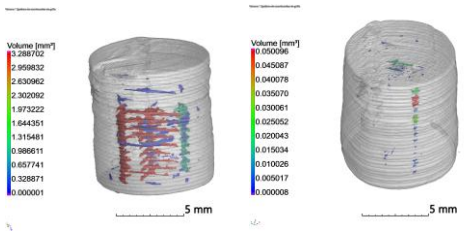

Figure 6. Tomographic reconstruction of the printed samples with a) low porosity and b) no porosity.

3.2 Debinding

As bio-based feedstocks are transformed from renewable element and not petroleum, their thermal degradation is carbon-neutral. Moreover, the basic binder we used does not contain solvable components and prohibits an intermediate solvent debinding step. A single thermal debinding will be used to debind the created parts.

A thermogravimetric analysis (TGA) is led on a sample with a 10°C·min^{-1} rate of heating in a NETZSCH STA 449C thermogravimetric analyser to observe at which temperature the binder is degrading.

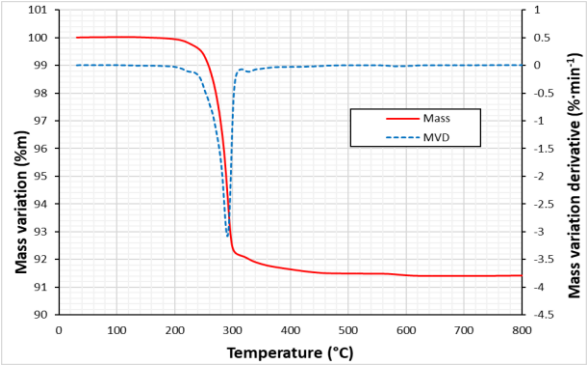

Figure 7. Thermogravimetric analysis of the feedstock between 100°C and 500°C. MVD stand for Mass variation derivative

Figure 7 shows the TGA and a loss of matter is observable from 200°C to 325°C, when the Derivative Mass is negative. The peak of degradation is centred around 291°C. A debinding cycle with a maximal temperature of 300°C will ensure a suitable debinding. A heating rate of 30°C·min^{-1} is applied and ensure that no defaults are created during the debinding step.

Commenté [CK3]: What was the heating rate in debinding? Did you use holding temperatures?

Debinding of the low and no porosity printed parts shows that the porosity plays a significant role during the debinding stage, as shown on figure 8. The absence of porosity prevent gas created during debinding to escape thus creating internal pores. On the other hand, the porosity of the low porosity sample did not expand nor change in shape. After debinding, the debinded part of printed sample having a low porosity has a porosity of 0.69%, whereas the debinded specimen of printed sample without porosity has a 3.89% porosity.

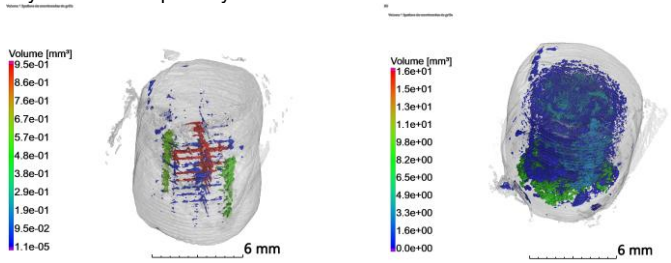

Figure 8. Tomographic reconstruction of the debinded samples prepared from printed sample with a) low porosity and b) no porosity.

3.3 Densification

The densification is done by conventional sintering, under a protective argon atmosphere. To determine the best sintering temperature of each sample, a dilatometry analysis from 50 to 1300°C is performed. The result of the dilatometry is presented in figure 9. The powder begins to sinter at 1100°C but phenomenon gain prevalence from 1225°C to 1260°C where the melting begins. The optimal sintering temperature is determined to be 1250°C.

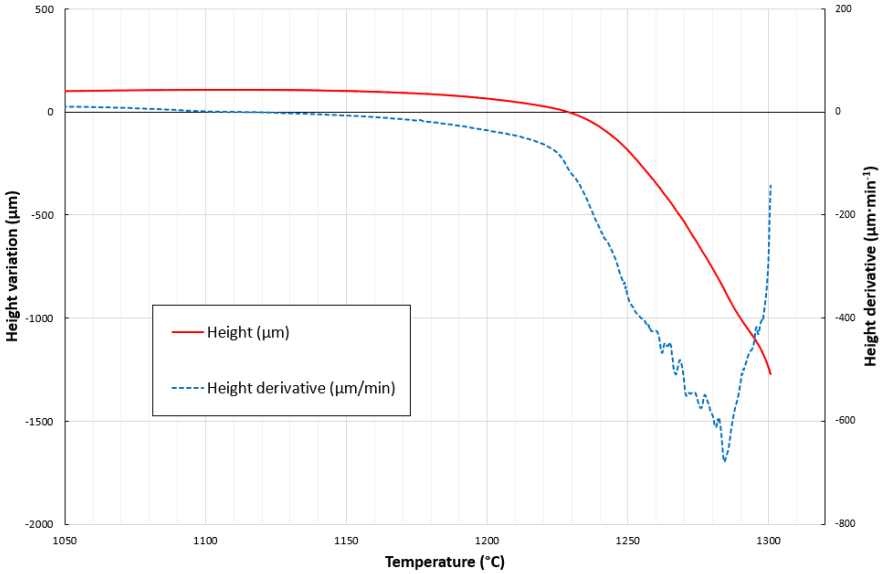

Figure 9. Dilatometric analysis of the powder under protective argon gas.

The debinded samples undergo a sintering cycle in the dilatometer with a start at 50°C, an increase to 1100°C at 50°C·min^{-1}, followed with an increase to 1250°C at 25°C·min^{-1} (to not exceed the set temperature), and a time at temperature of 2h followed by a decrease of temperature to room temperature at 50°C·min^{-1}.
The sample are then analysed with the tomograph and the results are presented in figure 10.

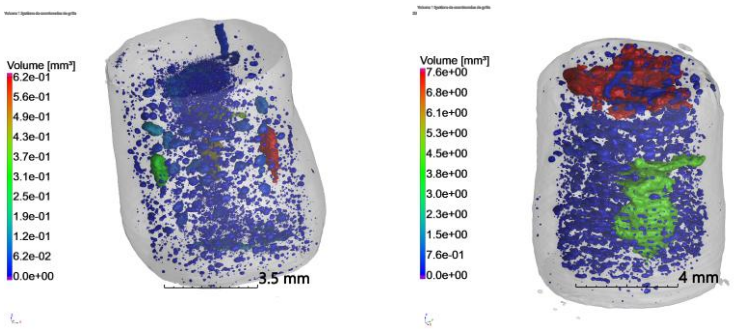

Figure 10. Tomographic reconstruction of the sintered samples prepared from printed samples a) with low porosity and b) no porosity.

The final porosity of the sintered sample from a printed sample with a low porosity is of 0.97% whereas the final porosity of the sintered sample prepared form a printed sample without porosity is larger at 35.9%. The sintering step aggravate the porosity agglomeration of the parts.

4. Conclusion

This work proved that a bio-based binder is suitable for the PIM-like EAM process, and final porosity obtained with conventional sintering are low (<1%) when the printing step is mastered.
The mastery of the printing step proves to be critical as the porosity need to be controlled and not eliminated to ensure that the debinding step does not create new pores.
A single powder was investigated during the study, but the whole process proved to be applicable for other materials.

For the binder created, prospects are to publish other results on different kind of materials and to continue to understanding the associated mechanisms at each step of the process in order to control them.

Acknowledgement
The research was supported by the EIPHI Graduate School (contract ANR-17-EURE-0002) including its experimental facilities (manufacture of the high loaded feedstock, printing and optical 3D metrology). The authors are grateful to MIFHySTO technological platform for the use of equipment. Some of the work in this article was created with the Renatech platform.

References
[1] GERMAN, Randall M., et al. Powder injection molding. 1990.
[2] ROYER, Alexandre, BARRIÈRE, Thierry, and GELIN, Jean-Claude. Development and characterization of a metal injection molding bio sourced Inconel 718 feedstock based on polyhydroxyalkanoates. Metals, 2016, vol. 6, no 4, p. 89.
[3] MELCHELS, Ferry PW, DOMINGOS, Marco AN, KLEIN, Travis J., et al. Additive manufacturing of tissues and organs. Progress in polymer science, 2012, vol. 37, no 8, p. 1079-1104.
[4] PENG, Erwin, ZHANG, Danwei, et DING, Jun. Ceramic robocasting: recent achievements, potential, and future developments. Advanced Materials, 2018, vol. 30, no 47, p. 1802404.
[5] VALINO, Arnaldo D., DIZON, John Ryan C., ESPERA JR, Alejandro H., et al. Advances in 3D printing of thermoplastic polymer composites and nanocomposites. Progress in Polymer Science, 2019, vol. 98, p. 101162.
[6] MAGUIRE, Alianna, POTTACKAL, Neethu, SAADI, M. A. S. R., et al. Additive manufacturing of polymer-based structures by extrusion technologies. Oxford Open Materials Science, 2021, vol. 1, no 1, p.itaa004.
[7] EYNDE, Michael Van den et PUYVELDE, Peter Van. 3D Printing of Poly (lactic acid). Industrial Applications of Poly (lactic acid), 2017, p. 139-158.
[8] DONG, J., TÜMER, N., PUTRA, N. E., et al. Extrusion-based 3D printed magnesium scaffolds with multifunctional MgF 2 and MgF 2–CaP coatings. Biomaterials Science, 2021, vol. 9, no 21, p. 7159-7182.
[9] JIANG, Dayue and NING, Fuda. Anisotropic deformation of 316L stainless steel overhang structures built by material extrusion based additive manufacturing. Additive Manufacturing, 2022, vol. 50, p. 102545.
[10] SINGH, Gurminder, MISSIAEN, Jean-Michel, BOUVARD, Didier, et al. Additive manufacturing of 17–4 PH steel using metal injection molding feedstock: Analysis of 3D extrusion printing, debinding and sintering. Additive Manufacturing, 2021, vol. 47, p. 102287.
[11] SANGYEUN, Park et al. Rapid manufacturing of micro-drilling devices using FFF-type 3D printing technology, Scientific Reports 11.1, 2021
[12] FAN, Yujiang, NISHIDA, Haruo, SHIRAI, Yoshihito, et al. Thermal degradation behaviour of poly (lactic acid) stereocomplex. Polymer Degradation and Stability, 2004, vol. 86, no 2, p. 197-208.
[13] PANDYA Shishir, RAMAKRISHNA K.S., ANNAMALAI Raja, UPADHYAYA Anish, Effect of sintering temperature on the mechanical and electrochemical properties of austenitic stainless steel, Materials Science and Engineering, 2012
[14] HANEMANN, Thomas and HELDELE, Richard, Fatty Acid Surfactant Structure–Feedstock Flow Properties: Correlation for High-Pressure Ceramic Injection Molding; 2011
[15] KONG, Xiangji, BARRIERE, Thierry, et GELIN, J. C. Determination of critical and optimal powder loadings for 316L fine stainless steel feedstocks for micro-powder injection molding. Journal of Materials Processing Technology, 2012, vol. 212, no 11, p. 2173-2182.
[16] JARDIEL, Teresa, SOTOMAYOR, Maria Eugenia, LEVENFELD, Belén, et al. Optimization of the Processing of 8-YSZ Powder by Powder Injection Molding for SOFC Electrolytes. International Journal of Applied Ceramic Technology, 2008, vol. 5, no 6, p. 574-581. International Journal of Applied Ceramic Technology, 5 (2008), pp. 574-581